machines

MDPI

Article

Simple Internal Model-Based Robust Control Design for a Non-Minimum Phase Unmanned Aerial Vehicle

Argyrios Zolotas

Autonomous Systems Dynamics and Control Research Group, Centre for Autonomous and Cyber-Physical Systems, SATM, Cranfield University, Cranfield MK43 0AL, UK; a.zolotas@cranfield.ac.uk

Abstract: Robust control has been successful in enabling flight stability and performance for UAVs. This paper presents a simple explainable robust control design for UAV platforms with non-minimum phase (NMP) zero characteristics in their model. The paper contributes to economic (simple) robust control design by addressing the NMP model's characteristics via Internal Model Control (IMC) and its impact on the UAV pitch response performance. The proposed design is compared with a Parallel Feedback Control Design (PFCD) scheme for the same vehicle platform, for fair comparison. Simulation results illustrate the achievement of the proposed control designs for the UAV platform; only the pitch control is addressed. A by-product of this work is the interpretation of different ways of manipulating the non-minimum phase plant model, so-called 'modelling for control', to enable the simple controller design. The work in this paper underpins the simplicity and robustness of the IMC technique for the NMP UAV platform, which further supports the explainability of the control structure relative to performance.

Keywords: unmanned aerial vehicles; robust control; explainability; non-minimum phase zero; time delays; internal model control

Citation: Zolotas, A. Simple Internal Model-Based Robust Control Design for a Non-Minimum Phase Unmanned Aerial Vehicle. *Machines* **2023**, *11*, 498. https://doi.org/10.3390/machines11040498

Academic Editors: Maria Eusebia Guerrero-Sanchez and Omar Hernández-González

Received: 28 March 2023
Revised: 11 April 2023
Accepted: 19 April 2023
Published: 21 April 2023

1. Introduction

Zeros are a fundamental aspect of systems and control, and there has always been a certain fascination with their unstable nature, or so-called non-minimum phase. Non-minimum phase zeros, if one describes them in a slightly exaggerated way, could be seen as "silent but lethal", given that they tend to be one of the worst features a dynamic system possesses (especially for designing simple linear control), albeit researchers developing control methodologies savour the design challenge presented by these kinds of zero characteristics [1].

Various practical systems have dynamics that exhibit non-minimum phase characteristics, from process control [2] (e.g., thermal processes where time delays are approximated by non-minimum phase zero system dynamics), to aerospace systems (e.g., altitude of an aircraft, tail-controlled missile) [3], to maritime systems (e.g., pitch control of underwater vehicles) [4], to mechanical systems (e.g., pole balancing type systems) and ground vehicle applications (e.g., nulling control of tilting rail vehicles) [5].

Non-minimum phase zeros, depending on their location on the s-plane, impose system performance challenges to designing effective controls. Non-minimum phase zeros, just like time delays, impose bandwidth constraints (i.e., limit the controller gain). The time domain response of an otherwise stable system with an odd number of non-minimum phase zeros initially moves in the opposite direction from the desired set point, before proceeding towards the set point direction. In fact, Åström discusses the limitations of control performance due to NMP zeros in his well-known article [6].

That control of UAV platforms to enable advanced air mobility applications [7,8], is of great interest, is not in doubt. The control literature includes a plethora of related work; we concentrate on more recent examples from the literature on the control of small

fixed-wing UAVs (with NMP zeros). From the more generic viewpoint of UAV dynamic control design, a very recent paper explores the implementation of of linear and nonlinear control methods for controlling an X3D quadrotor's intended translation position and rotation angles while hovering, including the design, implementation and evaluation of the controller's effectiveness [9]. Safwat et al. in [10] investigated a robust nonlinear flight control system for a small fixed-wing UAV against uncertainties and external disturbances, with a particular view towards GNC. Wang et al. in [11] concentrated on robust H-infinity attitude control for a quadrotor (modelling in 3D). The control of UAV platforms that exhibit non-minimum phase characteristics in their models is also addressed by the research community. Elkhatem et al. [12] explored a robust control approach (combining fractional-order and LQR) for a fixed-wing UAV platform with NMP zeros, also considering actuator faults. Both the UAV platform and the control approach are different from those proposed in this paper. Work in [13] concentrated on fixed-wing UAV platforms (with non-minimum phase zeros) and basic controllers via root locus; the authors followed a rigorous analysis approach in their paper. Both the UAV platform and the control approach are different from those proposed in this paper. Work in [14] discussed bicopters with NMP zeros but focused on designing H-infinity loop shaping control. From the references presented here, the interest in smaller UAV platforms is also evident.

To the best of the author's knowledge, this paper represents the first rigorous attempt to present classical Internal Model Control (IMC) design and its explainability in the context of small fixed-wing UAVs with non-minimum phase (NMP) zero characteristics, particularly for the UAV platform example considered here for attitude control.

IMC is a well-known inverse-based systematic controller design framework that seeks to strike a balance between system performance and robustness [15]. It is based on the Q-parametrisation (or Youla parametrisation) of all stabilizing controllers for a given dynamical system [16–18]. IMC is an attractive approach, building upon the simplicity of classical feedback control design for obtaining controllers that meet practical robustness and performance requirements. This paper leverages this feature for the attitude control of UAVs.

The current paper contributes to robust control design by addressing the UAV platform NMP model's characteristics via Internal Model Control (IMC). The particular emphasis is on the impact of the proposed simple control design solutions on the UAV pitch response performance. A by-product of the work is the suggestion of multiple ways of representing the non-minimum phase plant model, so called 'modelling for control', to assist the controller's design steps. The work in this paper underpins the simplicity and robustness of the IMC technique and its explainable controller structure linked to the UAV pitch control problem.

2. Methodology and Structure of The Paper

The design of simple and robust controllers for UAV systems, especially when their dynamics are affected by NMP zero characteristics, is still an open issue and is paramount for the maintenance of robustly stable dynamic operations of the vehicle platform. This enables safety in applications that UAVs are used for [19]. While there is a defined structure for flight control (auto-pilot architecture), the way controllers are designed also varies depending on the specific UAV platform technology (e.g., fixed-wing, rotors, VTOL, tail-sitters [20]). In addition, and in particular with the advent of AI/ML based control for UAVs, "explainable" control (design/solution) offers advantages [21]. The methodology of controller design also depends on the UAV technology/application, and not much work has been previously published regarding IMC control strategies for NMP UAV systems.

This paper proposes internal model-based robust control design in an explainable manner (here, we refer to explainability in the sense of how the considerations of modelling for control are linked to the controller design structure for the UAV attitude control problem and its relation to achieved performance/robustness), utilising the Internal Model Control philosophy for an NMP aerial vehicle platform. The performance of the controller is

assessed using simulations and is discussed alongside a recent PFCD proposed design for the same vehicle platform.

2.1. Methodology

The methodology followed in this paper is based on three main steps. Firstly, the (NMP) UAV model and its model representation (for control design) are presented. The control problem is that of controlling the UAV pitch angle.

The second step consists of controller synthesis. A two-degrees-of-freedom (DoF) IMC control method is followed, in order to benefit from its explainability relating to the designed controller structure. Finally, the proposed controllers are assessed and discussed alongside a recently proposed PFCD scheme for the same UAV platform.

Extensive simulations and discussion of the results are provided to evaluate the efficacy and extent of the performance benefits of the proposed solutions. The proposed solutions, given their explainable and simplified structure, provide an attractive framework for practising control engineers, i.e., a more direct method of "refined" classical control design for such UAV platforms.

2.2. Overview of Constraints Imposed by NMP Zeros on SISO Control Loop Shaping

Systems with NMP zeros impose challenging constraints on control system design. Åström discussed fundamental limitations on control performance in his European Journal of Control tutorial paper (the interested reader is referred to [6] for details). The discussion was limited to Single-Input–Single-Output (SISO) systems for an archetypal two-DoF (-ve) feedback control setup having loop TF $L(s) = P(s)C(s)$ (where $P(s)$ is the plant TF and $C(s)$ is the controller block). Bode's ideal loop shape (note that in general, n is considered fractional order and such a transfer function relationship is explored in fractional order control; however, fractional order control is not considered in this paper) was emphasised, i.e., a loop TF of the form $L_{bi}(s) = \left(\frac{s}{\omega_{\text{gc}}}\right)^n$ where ω_{gc} is the gain crossover frequency and n the slope of the amplitude curve (although this can be a somewhat conservative assumption, simplifying the analysis). The outcome was key results (inequalities) for the gain crossover frequency for minimum phase and non-minimum phase systems.

Here, we present only the *crossover frequency inequality* for NMP systems, with the same assumptions as in [6], for simplicity. In the equations below, $P(s) = P_{\text{mp}}(s)P_{\text{nmp}}(s)$ is the minimum phase/NMP plant factorisation, with $|P_{\text{nmp}}(j\omega)| = 1$ and $\arg P_{\text{nmp}}(j\omega)$ being negative. The achievable bandwidth is characterised by the gain crossover frequency, referred to as ω_{gc}. The NMP system's *crossover frequency inequality* is

$$\arg L_(j\omega_{\text{gc}}) = \arg P_{\text{nmp}}(j\omega_{\text{gc}}) + \arg P_{\text{mp}}(j\omega_{\text{gc}}) + \arg C(j\omega_{\text{gc}}) \geq -\pi + \phi_{\text{m}}$$

where ϕ_{m} is the Phase Margin. Taking $P_{\text{mp}}(s)C(s)$ as equal to Bode's ideal loop TF,

$$\arg P_{\text{nmp}}(j\omega_{\text{gc}}) + \arg C(j\omega_{\text{gc}}) \approx n_{\text{gc}}\frac{\pi}{2},$$

hence, the inequality becomes

$$\arg P_{\text{nmp}}(j\omega_{\text{gc}}) \geq -\pi\left(1 + \frac{n_{\text{gc}}}{2}\right) + \phi_{\text{m}}$$

where n_{gc} is the slope of the loop TF at the gain crossover frequency. The typical upper bound of achievable crossover frequency for a system with a single NMP zero at location $s = z_+$ will be

$$\frac{\omega_{\text{gc}}}{z_+} \leq \frac{1}{2}\tan\left(\pi\left(1 + \frac{n_{\text{gc}}}{2}\right) - \phi_{\text{m}}.\right)$$

Note that it is more challenging to control systems with slow NMP zeros (as bandwidth decreases with decreasing zero frequency); similarly, time delays impose an upper bound

on achievable bandwidth [6]. This section presents the importance of NMP zeros and their location in dynamical systems, especially from an LTI viewpoint.

2.3. Structure of the Paper

The paper is structured as follows: In Section 3, we present the model of the system and describe its various representations (i.e., modelling for control) for synthesizing controllers. In Section 4, we describe the control design setup, and briefly introduce the PFCD approach from [22] which is used for comparisons with the proposed scheme. Section 5 presents the proposed Internal Model Control (IMC) design. We present the results of the proposed controllers alongside the PFCD strategy for the same model in Section 6, and draw conclusions on the presented work in Section 7.

3. UAV Platform and Modelling for Control

The UAV system model utilised for the work is a tailless UAV (with elevon control surfaces) and was proposed in [23]. The schematic of the UAV and its directions can be seen in Figure 1.

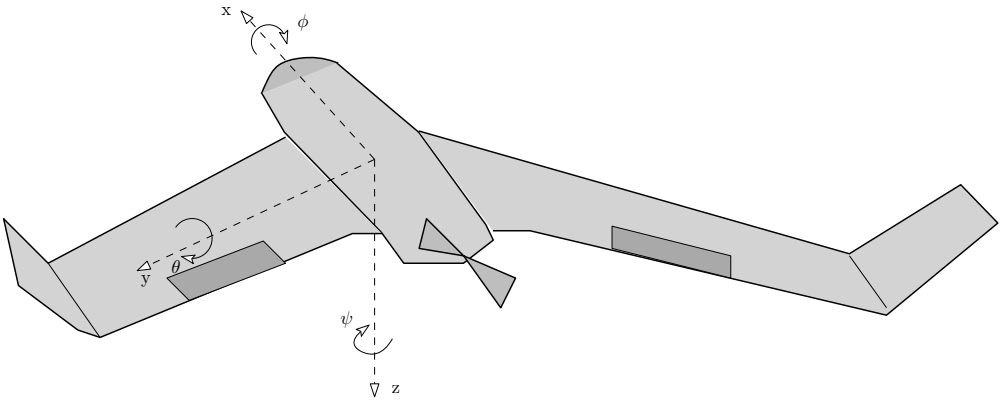

Figure 1. UAV schematic (elevons on wings shown in darker grey shade).

The UAV model has been extensively reported in [23] (the interested reader can refer to the paper for more details). For completeness, we state the basic UAV structure here: the wingspan is 1.2 m, the sweep angle is 30 deg, UAV length is 0.45 m and UAV weight is approx. 0.85 kg. Brushless motors are the propulsion mechanisms, enabling speeds of up to about 25 m/s. Pitch and roll manoeuvring is enabled by two elevons.

The pitch and roll system dynamics for the UAV platform were obtained using system identification via experiments (a PixHawk flight controller was used in the experiments by the authors). The assumptions made by the authors in their paper [23] were: (i) the UAV is moving at a given speed with respect to the ground, (ii) the longitudinal and lateral dynamics are considered to be decoupled, (iii) a linear model in the vicinity of the operating condition applies.

In this paper, we concentrate specifically on the control of the UAV pitch response, given its important NMP zero characteristics. A system identification analysis in [23] showed that a second-order TF with a time delay was sufficient to characterise the pitch response of the UAV (a similar TF structure also applies for the roll response, but including minimum phase zero; however, roll control is not considered in this work. Of course, the proposed control concepts can be followed for the roll response control problem, which poses fewer performance constraints due to not having NMP zero characteristics); with control input, the normalised elevons command δ_e and output the pitch rate q. For the system identification details, the interested reader is referred to [23]. The transfer function is given below:

$$Q_d(s) \equiv \frac{Q(s)}{\Delta_e(s)} = \frac{(-106.2s + 677)e^{-0.0632s}}{s^2 + 13.69s + 416.7} = \frac{1.6247(1 - 0.1569s)}{(1 + 0.0329s + 0.0024s^2)}e^{-0.0632s}. \quad (1)$$

Equation (1) (note that in the case of the pitch angle response, $\Theta_{\delta_e}(s) = s^{-1}Q_{\delta_e}(s)$) presents the pitch rate transfer function in time-constant format. Such a representation is not the norm in transfer function modelling of aerospace vehicle models, but it is useful here to illustrate the importance of the various time constants in the model. Note that all closed-loop simulations are performed using the original model from [23], with the actual time delay (see (1)). However, controllers are designed based on relevant so-called"modelling for control" approximations. Moreover, note that the time delay in the original model is defined by the sampling used in experiments of model identification (i.e., a slower sampling time results in an increased time delay). For the UAV platform, the frequency range of interest is between 2 and 40 rad/s.

Modelling for Control

The work in this paper also contributes to ways of representing the transfer function $Q_d \equiv \frac{Q(s)}{\Delta_e(s)}$ for control design (the pitch rate TF is discussed here, as it is used to design the control for the rate feedback). Different plant model representations enable flexibility in controller design; this is advantageous via the IMC method, which results in controller structures of varying complexity, with simple controller architecture being favourable in terms of "explainability" and easier for practical implementation. While the discussion here is on the pitch rate channel, we also present a special case of manipulation of the model for the pitch angle channel.

Below, we present a series of Q_d TF versions in time-constant format (this is currently a usual practice in process control design, especially when it comes to IMC control method applications [24]). Specifically, we present different ways in which the non-invertible portion of the TF model can be represented for control design. For visualisation purposes, the Pole-Zero (PZ) maps of the different TF model versions are shown in Figure 2, while the step (to unity amplitude step input) responses are listed in Figure 3a,b (the latter for the Pade approximations) for easy viewing.

- Pade approx. 1st order of Q_d:

$$Q_{dp1}(s) = \frac{1.6247(1 - 0.1569s)(1 - 0.0316s)}{(1 + 0.0316s)(1 + 0.0329s + 0.0024s^2)}. \quad (2)$$

- Pade approx. 2nd order of Q_d:

$$Q_{dp2}(s) = \frac{1.6247(1 - 0.1569s)(1 - 0.0316s + 0.00033s^2)}{(1 + 0.0316s + 0.00033s^2)(1 + 0.0329s + 0.0024s^2)}. \quad (3)$$

- Pade approx. 3rd order of Q_d:

$$Q_{dp3}(s) = \frac{1.6247(1 - 0.1569s)(1 - 0.01361s)(1 - 0.018s + 0.00016s^2)}{(1 - 0.01361s)(1 + 0.018s + 0.00016s^2)(1 + 0.0329s + 0.0024s^2)}. \quad (4)$$

- Overall time delay (combined NMP zero approx. as time delay and original time delay):

$$Q_{ds1}(s) = \frac{1.6247}{(1 + 0.0329s + 0.0024s^2)} e^{-0.22s}. \quad (5)$$

- Rational approximation of Q_{ds1} (Taylor expansion) to pure NMP zero:

$$Q_{ds2}(s) = \frac{1.6247(1 - 0.22s)}{(1 + 0.0329s + 0.0024s^2)}. \quad (6)$$

- Approx. original time delay by first-order Taylor expansion as extra NMP zero:

$$Q_{ds3}(s) = \frac{1.6247(1 - 0.0632s)(1 - 0.1569s)}{(1 + 0.0329s + 0.0024s^2)}. \quad (7)$$

- Take (5) and represent worst case time delay as slow pole approximation:

$$Q_{ds4}(s) = \frac{1.6247}{(1 + 0.22s)(1 + 0.0329s + 0.0024s^2)}. \quad (8)$$

- Take Q_d and represent only the pure time delay as slow pole approximation:

$$Q_{ds5}(s) = \frac{1.6247(1 - 0.1569s)}{(1 + 0.0632s)(1 + 0.0329s + 0.0024s^2)}. \quad (9)$$

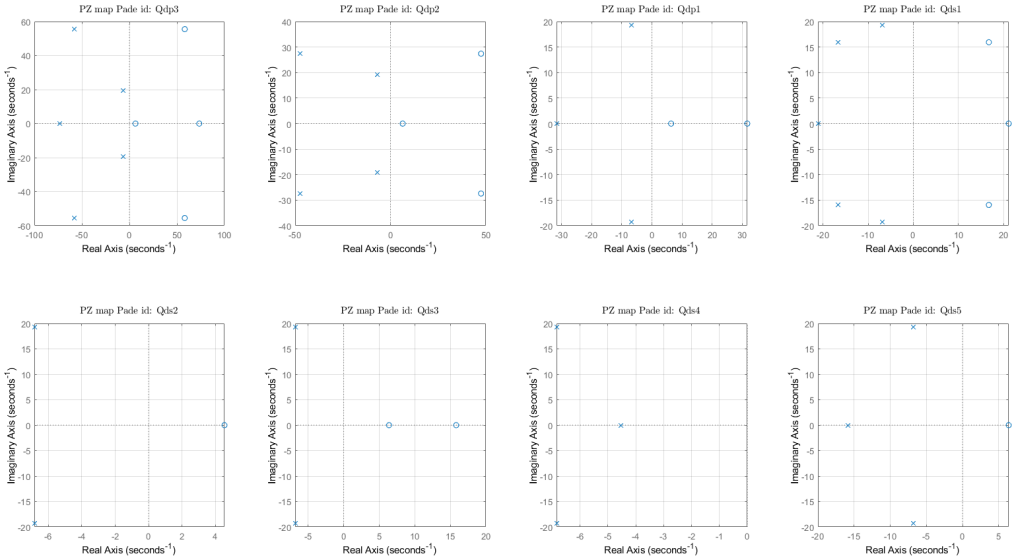

Figure 2. Pole–zero map of the various Q_d (pitch rate) TF versions.

Clearly, the TF (order) complexity (numerator, denominator polynomial order; rational and/or non-rational elements included) varies, with this resulting in controllers of varying complexity via Direct Synthesis (DS) or model-based control methods [25].

A comparison of the frequency responses (Bode magnitude and phase plots) of the different TF models is shown in Figure 4. This is important as it illustrates how the non-compensated system stability margins vary with the manipulation of the TF model and the trade-off between simplicity and conservativeness introduced in the different TF model versions (compared with the original model). The characteristics of the different plant TF models are detailed in Table 1.

Modelling for control is an important step in IMC designs, and from the comparison, Q_{dp3} seems the better approximate representation of the original TF Q_d; however, the Q_{dp3} structure complexity (numerator, denominator polynomial order) will map to the model-based controller design. The Plant TF simplification id: Q_{ds2} shows good agreement (phase plot) up to around a frequency of 10 rad/s, while introducing GM conservativeness (this is due to the virtually slower NMP zero introduced by combining the original NMP zero and the NMP zero approximation of the time delay). To maintain a rational model TF with the smallest possible numerator and denominator polynomials, Q_{ds2} is the representation selected for controller design. (Note that the pitch angle TF can be obtained by integrating the pitch rate.)

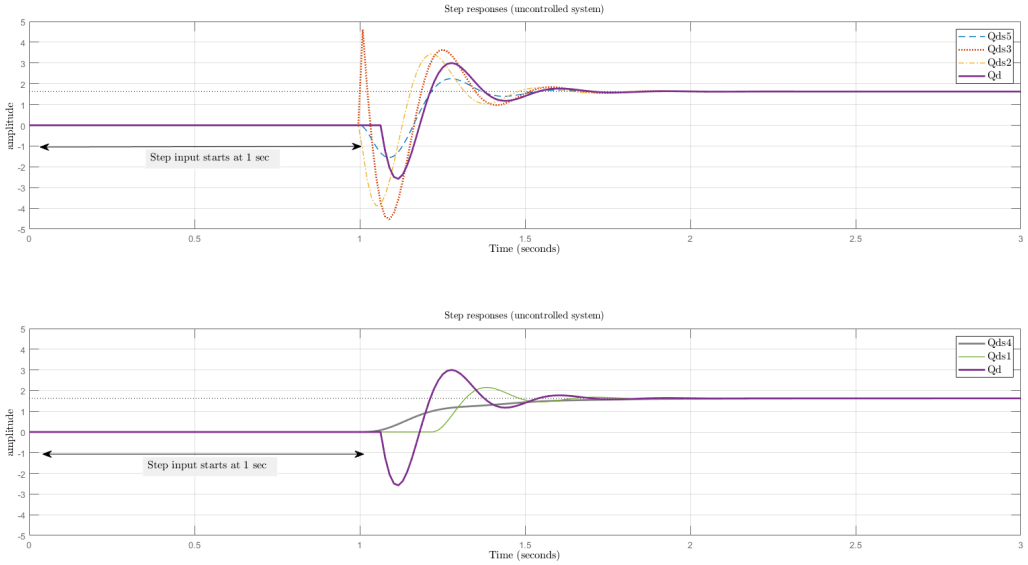

(**a**) Response to normalised unit step elevon input (approximated versions; no control yet).

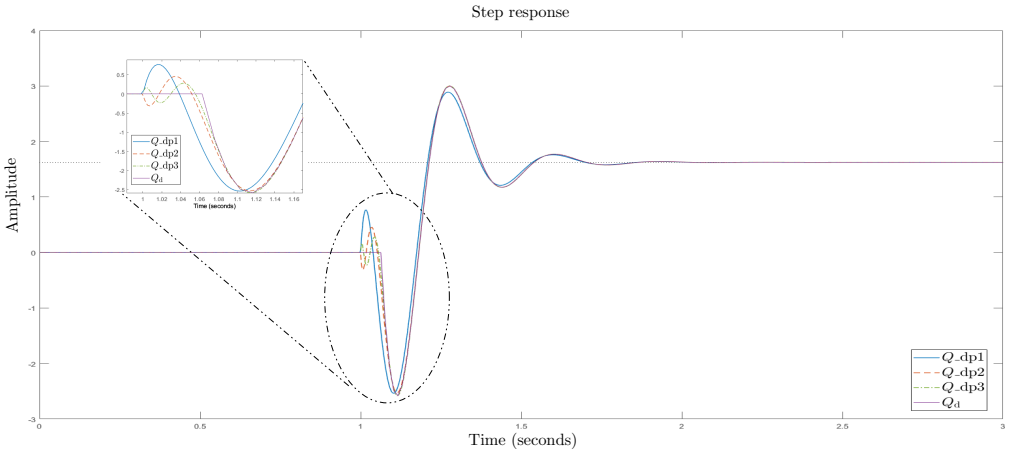

(**b**) Response to normalised unit step elevon input (Pade approximation versions; no control yet).

Figure 3. Step response comparison of model simplifications for the pitch rate transfer function Q_d.

Table 1. Q_d (no controller included yet) model representation results.

	Response Indexes				
TF	**OS/US**	T_s	T_r	**PM**	**GM**
	[%]	**[sec]**	**[sec]**	**[deg]**	**[dB]**
Q_d	84.6 OS	0.812	0.025	−115@109 rad/s	−3.08@78.8 rad/s
Q_{dp1}	77.8 OS	0.802	0.203	133@109 rad/s	−16.8@16.4 rad/s
Q_{dp2}	84.4 OS	0.822	0.188	19.2@109 rad/s	1.8@133 rad/s
Q_{dp3}	84.8 OS	0.812	0.206	−58.1@109 rad/s	−2.48 @83.9 rad/s
Q_{ds1}	32.6 OS	0.763	0.067	10.5@30.8 rad/s	0.506@31.5 rad/s
Q_{ds2}	111 US	0.765	0.02	−83@151 rad/s	−20.7@21.9 rad/s
Q_{ds3}	313 OS	0.802	-	-	−20.7@17.2 rad/s
Q_{ds4}	-	0.88	0.447	111@6.6 rad/s	6.94@21.9 rad/s
Q_{ds5}	38 OS	0.662	0.043	−130@43.6 rad/s	−14@17.2 rad/s

(1) OS: Overshoot; US: Undershoot; T_s, T_r settling, rise time; PM/GM: Phase margin/Gain margin (negative: reduction margins) for pitch rate feedback closure. (2) Unit step time-domain response for pitch rate. (3) Q_{ds3} due to initial kick in the response, negligible T_r, and due to phase advance nature, no PM. (4) Q_{ds4} no OS due to slow pole characteristics. (5) The equivalent TF for pitch angle Θ_d followed by multiplication with s^{-1}.

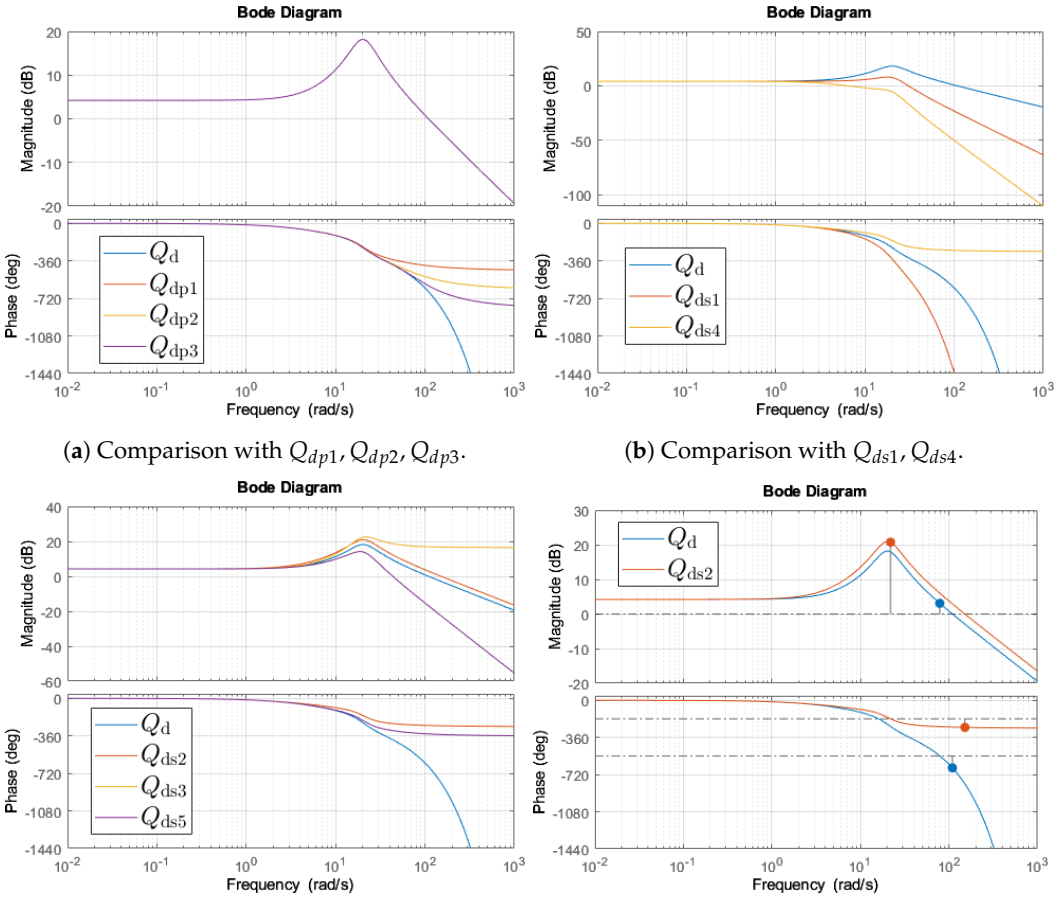

(**a**) Comparison with $Q_{dp1}, Q_{dp2}, Q_{dp3}$.

(**b**) Comparison with Q_{ds1}, Q_{ds4}.

(**c**) Comparison with $Q_{ds2}, Q_{ds3}, Q_{ds5}$.

(**d**) Margins of Q_d, Q_{ds2}.

Figure 4. Frequency response comparison of model versions for the pitch rate TF Q_d.

4. The Feedback Control Setup

Two-degrees-of-freedom controller design is at the heart of this paper. Here, the generic 2-DoF feedback (with reference feedforward) control setup is presented and forms the basis for the proposed UAV-targeted (pitch) control design. Note that the proposed control approach is compared with a recently proposed PFCD design for the same UAV example by [22]. The PFCD setup of [22] is briefly discussed, as it is used only for comparison purposes.

4.1. Generic 2-DoF Control Setup Preliminaries

The generic 2-DoF control setup (with reference feedforward) is shown in Figure 5.

As shown in Figure 5, we can use the following options to design the $K_{\mathrm{ff,r}}(s)$ (feedforward) and $K_{\mathrm{f}}(s)$ (feedback) controllers independently [26,27]:

$$K_{\mathrm{ff,r}}(s) = G_{yu\_}^{-1}(s)F_{\mathrm{r}}(s); \quad K_{\mathrm{pf,r}}(s) = G_{yu_+}(s)F_{\mathrm{r}}(s)$$

$G_{yu\_}(s)$ is the invertible and $G_{yu_+}(s)$ the non-invertible part of the plant (the plant is factorised as $G_{yu}(s) = G_{yu\_}(s)G_{yu_+}(s)$). The portion $F_{\mathrm{r}}(s)$ is included to guarantee that $K_{\mathrm{ff},r}(s)$ is a proper TF. In the case of "ideal feedforward", $K_{\mathrm{ff,r}}(s) = G_{yu}^{-1}(s)$, $K_{\mathrm{pf},r}(s) = 1$. The concept of reference command feedforward is used here.

In term of robustness, again referring to Figure 5,

$$E = \underbrace{S\left(K_{\mathrm{pf,r}} - G_{yu}K_{\mathrm{ff,r}}\right)}_{S'_{\mathrm{ff,r}}} R - SD \tag{10}$$

(s) dropped for simplicity, with $S = (1 + G_{yu}K_{\mathrm{f}})$ the sensitivity function, while $S'_{\mathrm{ff,r}}$ is the *feedforward sensitivity* for the rate. $K_{\mathrm{pf,r}}$, $K_{\mathrm{ff,r}}$ selection is performed to enable independent feedback and feedforward controller design, with the ideal feedforward $S'_{\mathrm{ff,r}} = 0$. Feedback control, performance-wise, is effective as far as $\|S\| < 1$; similarly, $\|S'_{\mathrm{ff,r}}\| < 1$ denotes feedforward effectiveness in improving performance [27].

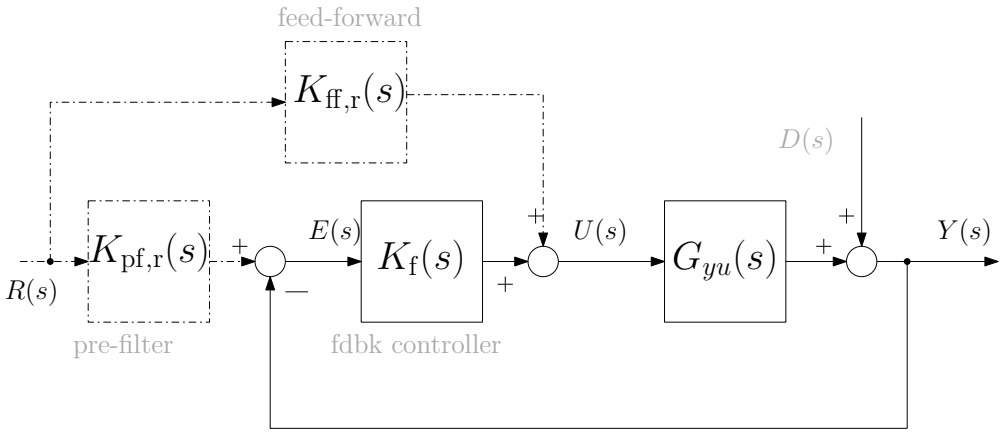

Figure 5. Typical 2-DoF feedback control framework.

4.2. Proposed Feedback Control Scheme for the UAV Platform Example

The proposed feedback control setup for the UAV platform is shown in Figure 6, with feedforward on the pitch rate loop and a simple pitch angle controller completing the outer loop. An optional feedforward for the pitch angle is also shown, for completeness. The proposed scheme is based on the 2-DoF approach, and Figure 6 allows for independent design of the relevant UAV-targeted feedback controllers (for the pitch rate controller, and as an option for the pitch angle controller). The feedback controllers are designed via the IMC method.

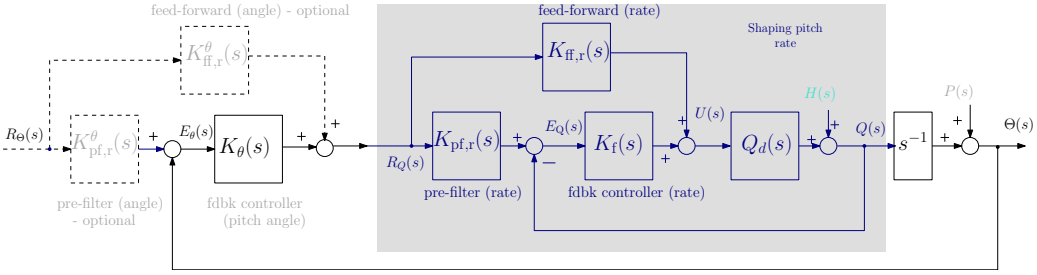

Figure 6. UAV pitch angle control loop (disturbance channel is shown) for the proposed control approach.

4.3. Parallel Feedback Control Design (PFCD) for Comparison

PFCD was originally discussed in [28], and a PFCD-based design for this specific UAV system model was presented in [22]. We compare the results of the proposed IMC-based design with the design outcome from [22]. The authors designed the following feedback control elements: $G_{yu}(s) = \frac{-106.2s+677}{s^2+13.69s+416.7}$; $C_{\mathrm{apf}}(s) = \mathrm{e}^{-0.0632s}$ (links to the plant rather than the controller); $\mathrm{sgn}() = +1$.

$$C_{\mathrm{qpf}}(s) = s\frac{1.4199}{0.01s+1}; K_{\mathrm{fcq}}(s) = \frac{0.3085(s+0.0032)}{s}; K_{\mathrm{ffq}}(s) = 0.01; K_{\mathrm{fc}}(s) = 2.5$$

The relevant time-domain and sensitivity plot (freq. domain) response results for PFCD are shown in Figure 7, in the results section (for the purpose of comparison is shown in Figure 8, with the proposed controller approach).

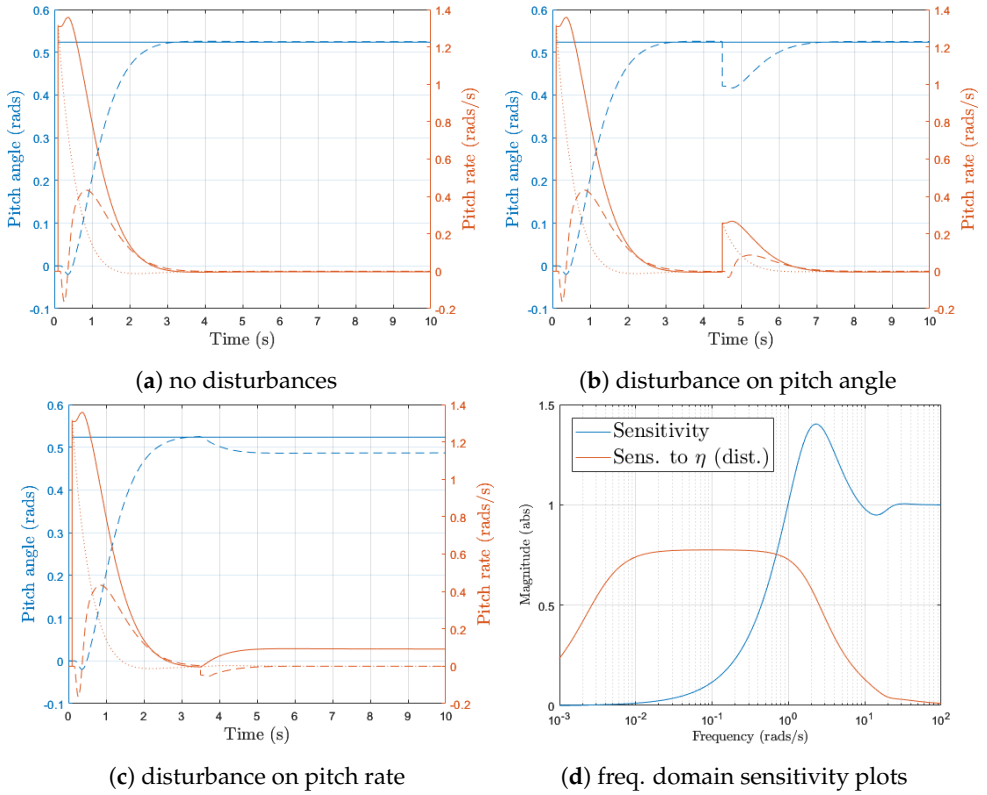

(**a**) no disturbances (**b**) disturbance on pitch angle

(**c**) disturbance on pitch rate (**d**) freq. domain sensitivity plots

Figure 7. PFCD time domain response (disturbances applied independently).

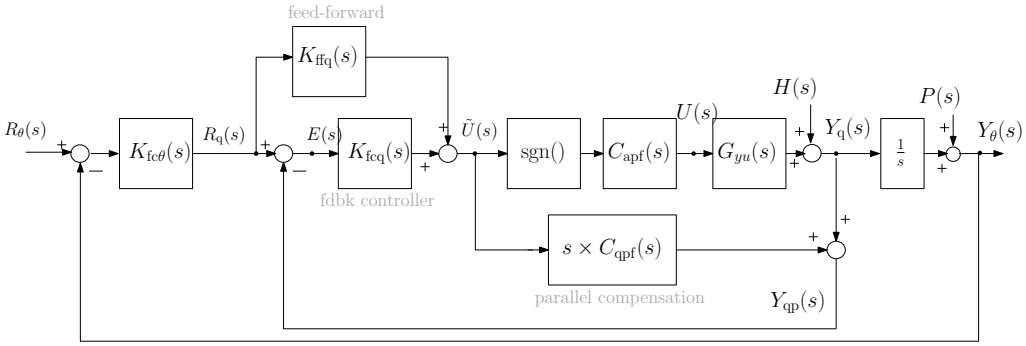

Figure 8. The PFCD architecture control feedback setup (adapted from [22]), for comparison.

5. Internal Model NMP Zero UAV-Targeted Control Design

5.1. Internal Model Control in a Nutshell

Internal Model Control (IMC) is a systematic controller design framework that uses an inverse-based approach to address a system's performance and robustness [15]. The popularity of IMC is evident in its frequent application in process control, particularly in the tuning of complex PID control loops [29–31]. Examples of IMC's effectiveness include its use in control problems with time delays [32] and in feedforward control for disturbance attenuation [33]. IMC formulations vary and include SISO and MIMO formulations [34], continuous- and discrete-time approaches [35], and linear and nonlinear methods [36,37], as well as bespoke IMC structures for fault-tolerant control (e.g., generalised IMC) [38]. In this paper, we focus primarily on the SISO linear control approach.

Utilizing plant (model) information is important in IMC design, and it involves the investigation of the plant transfer function structure to enable explainability for the control design (i.e., how the model structure selection impacts performance). For very complex models, appropriate model reduction techniques are necessary. Rivera [39] presented a rigorous perspective on model reduction within an IMC framework, while Skogestad [24]

proposed simple rules for model reduction and PID controller tuning in process control industry examples. The design principles of IMC have been developed through experience and lessons learned, mainly in process control applications. Mechanical or electromechanical natural systems, such as those in the aerospace vehicle control domain, typically with oscillatory modes, present a unique challenge compared with process control systems. IMC design for such systems can be informed by process control principles and good practice.

In terms of IMC-related applications to UAV systems, few can be found in the current literature; these relate both to rotors and fixed-wings. In particular, Bouzid et al, in their work [40], looked into the equivalence of IMC and PI control structures by proposing an IMC filter to ensure PI structure. The authors applied their proposed approach to a quadrotor trajectory-following problem with atmospheric disturbance. Work in [41] addressed a quadrotor attitude-control problem, comparing various IMC-PID control tuned versions, i.e., Chien–Hrones–Reswick, Cohen–Coon, and Ziegler–Nichols-based controllers. Gao et al. [42] proposed, again for a quadrotor UAV, a combined IMC and tracking differentiator approach for robust attitude control and trajectory tracking. Chen and co-authors, in their paper, proposed an adaptive IMC approach and used a fixed-wing UAV landing control problem example to illustrate their proposed approach [43]. The aforementioned papers are rather different to the approach taken in this one, which concentrates on the more classical control interpretation of IMC. Moreover, the available papers with some links to IMC for UAV systems do not extensively discuss methods of TF model representation in the design stages. Additionally, no work discussing the explainability of IMC control structure for such a UAV platform exists. These are the areas that this paper strongly contributes to.

Figure 9 illustrates the IMC feedback setup, where G_{yu} is the actual plant and $\tilde{G}_{yu}$ the model representation. In the figure, the disturbance input channel is also shown. We can start by setting $\tilde{G}yu = Gyu$, although this model will normally be an approximation of the true plant. It is important to note that we can design the feedback controller and feedforward control sections independently, as discussed earlier.

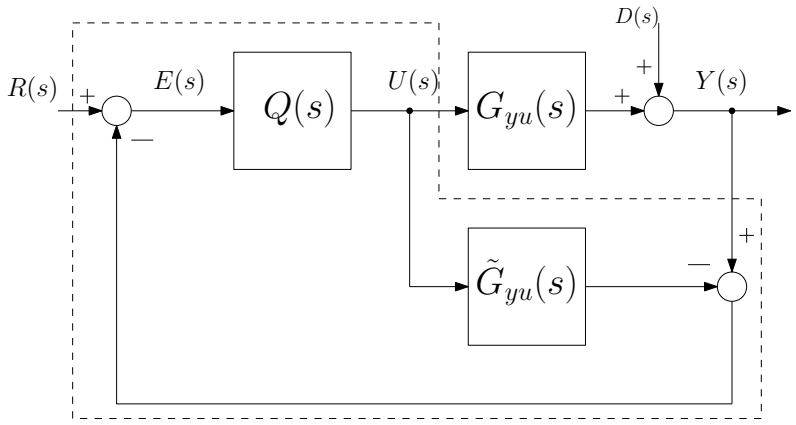

Figure 9. IMC feedback control setup ($Q(s)$ IMC filter).

We can summarise the design approach for IMC in the following way: the plant (model) is divided into two parts, the first part being minimum phase (invertible), while the second part contains non-invertible elements, such as non-minimum phase zeros and/or delays. These two parts can be represented as follows:

$$G_{yu}(s) = G_{yu_+}(s)G_{yu\_}(s) \tag{11}$$

with $G_{yu\_}(s)$ as the minimum-phase (i.e., invertible) model for the control portion, and $G_{yu_+}(s)$ the portion that is non-invertible. Hence, based upon model inversion, the IMC filter $Q(s)$ is selected as

$$Q(s) = G_{yu\_}^{-1}(s)F(s) \tag{12}$$

$F(s)$ facilitates the properness properties of the filter, and a common choice is $F(s) = \frac{1}{(\tau_f s+1)^n}$, which guarantees the properness of $Q(s)$ by selecting n and a tunable time constant τ_f for controller design (although integrating processes require slightly different considerations, as seen in [44]). This is used as a starting design point, but for oscillatory systems, $F(s)$ may need to include damped modes via a pole/zero combination for properness (note that this will increase the structure complexity). The classical feedback controller equivalent (represented in the dashed box in Figure 9) can be derived as follows:

$$\begin{aligned} K_f(s) &= Q(s)\left[1 - G_{yu}(s)Q(s)\right]^{-1} \\ &= G_{yu\_}^{-1}(s)F(s)\left[1 - G_{yu}(s)G_{yu\_}^{-1}(s)F(s)\right]^{-1} \\ &= G_{yu\_}^{-1}(s)F(s)\left[1 - G_{yu_+}(s)F(s)\right]^{-1} \end{aligned} \tag{13}$$

The structure of $F(s)$ will undoubtedly add to the complexity of the feedback controller $K_f(s)$. Note that time delays in (13) are approximated by a first-order Taylor expansion. Considering ideal conditions, $F(s)$ defines a "model reference" response.

5.2. IMC Control with No Rate Feedback

We start by presenting a single-feedback-loop strategy using the pitch angle output only (the control setup for this approach is the same as shown in Figure 6 with the grey area box set to $Q_{\delta_e}(s)$). Applying IMC will lead to a simple $P + I$ type feedback controller for the pitch angle loop. The plant TF in this case is

$$\begin{aligned} \Theta_d(s) = s^{-1}Q_{\delta_e}(s) &= \frac{-106.2s + 677}{s(s^2 + 13.69s + 416.7)}\mathrm{e}^{-0.0632s} \\ &= \frac{1.6247(1 - 0.1569s)}{s(1 + 0.0329s + 0.0024s^2)}\mathrm{e}^{-0.0632s}. \end{aligned} \tag{14}$$

Equation (14) presents the pitch angle transfer function (TF) in time-constant format. Note that this TF is of integrating form. Due to its integrating TF nature, a simplified approximation (here, we add the RHP-zero $z = \frac{1}{0.1569}$ as extra time delay; the denominator polynomial $(\tau^2 s^2 + 2\xi\tau s + 1)$ is approximated by $(\tau s + 1)^2$ ($\tau = 0.05$), then τ is injected as an extra time delay (partially following the approach in [24])) in the form of a pure integral with a time delay is

$$\tilde{\Theta}_d(s) = \frac{1.6247}{s}\mathrm{e}^{-0.27s}. \tag{15}$$

The above approximation is in the form $\tilde{G}_{\mathrm{ix}}(s) = \frac{k_1'\mathrm{e}^{-\tilde{\theta}_1' s}}{s}$ for the pitch angle, and, using the IMC process, a P + I type controller (i.e., a special case of a first-order system with delay, but with time constant $\to \infty$) is formed. Note that the invertible part of $\tilde{G}_{\mathrm{ix}}(s)$ is the portion excluding the delay. For completeness, the Bode plots for TF (14) and (15) can be seen in Figure 10. The IMC-based PI controller is thus given by

$$C_{\mathrm{PI}_1}(s) = \frac{1}{k_1'(\tau_c + \tilde{\theta}_1')}\left(1 + \frac{1}{4(\tau_c + \tilde{\theta}_1')s}\right) \tag{16}$$

with the integral time constant obtained from simple SIMC (Skogestad IMC) rules [24] (this is sometimes referred to as SIMple Control).

$$\tau_I = 4(\tau_c + \tilde{\theta}_1') \tag{17}$$

In the case of PI controller design, τ_c is the only design parameter that needs tuning. Its initial value is set to the given effective delay, i.e., $\tilde{\theta}'1$. Increasing τ_c results in a more robust, but slower, response. We use the 2-DoF design setup, as shown in Figure 5, with the

transfer function (15) used for the feedforward and pre-filter, i.e., $K_{\mathrm{ff,r}}$, $K_{\mathrm{pf,r}}$. Note that assuming "perfect control" yields

$$Y(s) = K_{\mathrm{pf,r}} R(s) \tag{18}$$

The following selection applies for the 2-DoF IMC pitch control design ((s) is dropped for simplicity)

$$F_r = \frac{1}{1 + 0.3825s + 0.05063s^2}; \quad \begin{array}{l} K_{\mathrm{ff,r}} = \tilde{\Theta}_d^- F_r, \\ K_{\mathrm{pf,r}} = \tilde{\Theta}_d^+(s) F_r \end{array} \tag{19}$$

F_r assumes a desired CL pitch angle step response settling time of approx. 1 s and 0.85 damping (it also avoids having an all-pass pre-filter), while $\tilde{\Theta}_d^-$ and $\tilde{\Theta}_d^+$ follow from the above considerations. The former is the invertible part of $\tilde{\Theta}_d$; the latter is set to $(1 - 0.27s)$ for rational TF. Under ideal conditions, one expects pitch angle track following with a settling time of around 1 s. Closed-loop response results for different τ_c are shown in Figure 11 (one can see that $\tau_c \approx 0.27$ s provides appropriate tracking performance). Figure 12 presents the frequency domain results for this simple approach, i.e., a CL sensitivity plot (including feedforward sensitivity) and robustness achievement (a Nyquist plot).

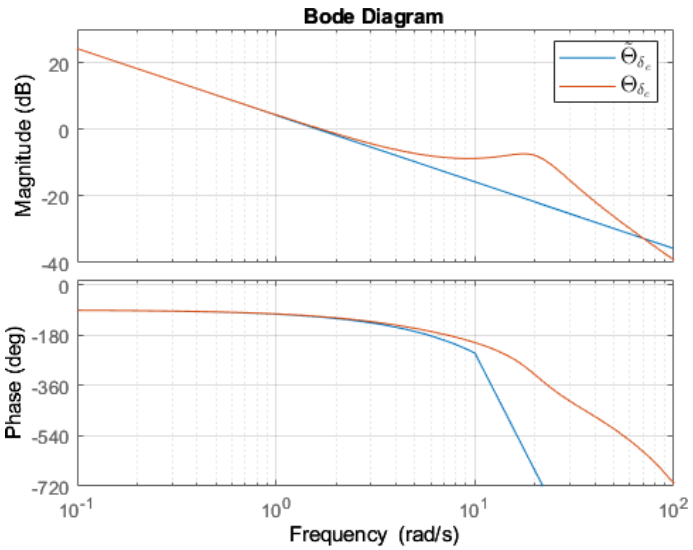

Figure 10. Comparing Bode plots of plant model (14) (red) and (15) (blue).

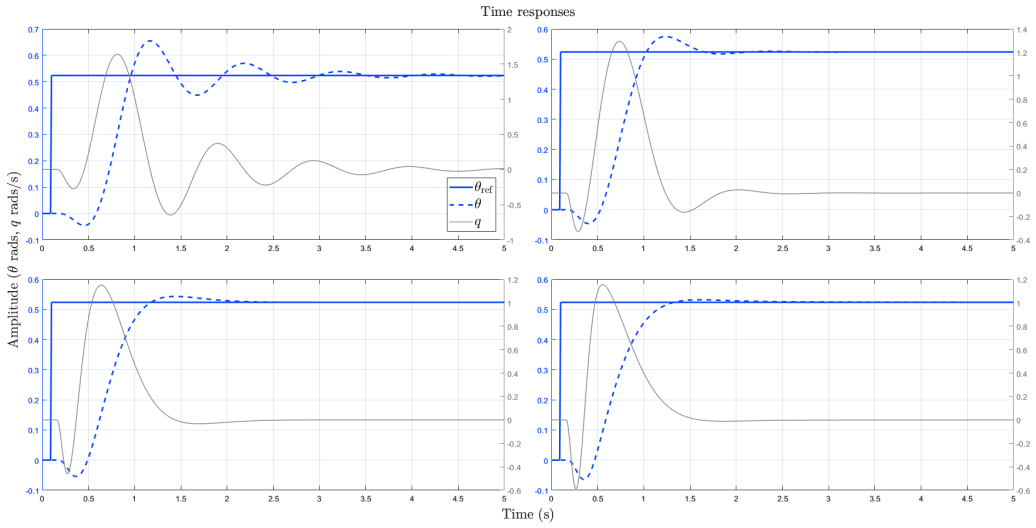

Figure 11. IMC–s time domain resp. (top-left, clockwise): $\tau_c = 0.0675$ s, 0.135 s, 0.54 s, 0.27 s.

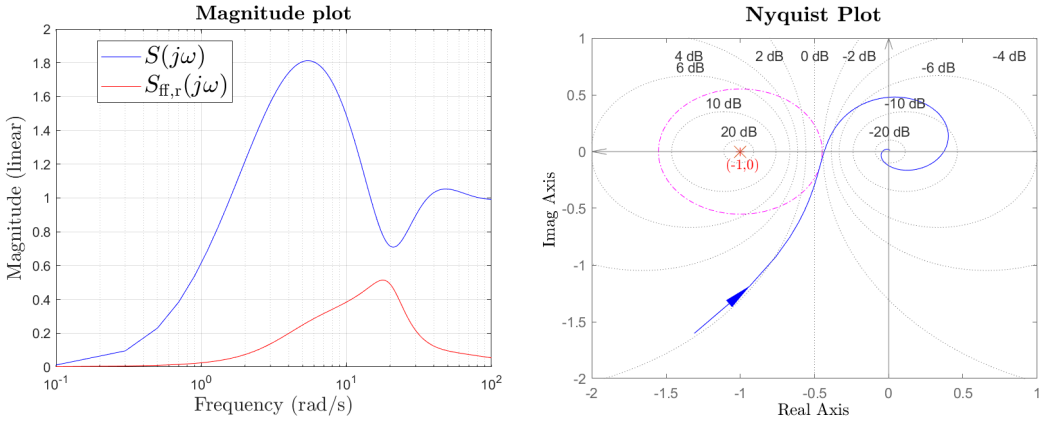

(**a**) Sensitivity plots (**b**) Nyquist plot

Figure 12. Closed–loop frequency domain results for IMC–s with $\tau_c = 0.27$ s.

5.3. IMC Control with Inner Loop (Pitch Rate Feedback) Included

Traditionally, a cascaded control design is executed for UAV systems, i.e., a pitch rate feedback for the inner loop and then an outer loop pitch angle feedback (note that the typical inner-loop based approach was also followed in [22]).

The feedback control setup is shown in Figure 6, with the emphasis of the feedforward on the pitch rate loop, while a simple pitch angle controller completes the outer loop (however, the scheme also shows optional feedforward and pre-filter blocks for the pitch angle). Note that, as mentioned earlier, the setup in Figure 6 allows for independent design of the feedback controller.

The IMC-based design begins by considering the pitch rate (inner loop) feedback, i.e., in a 2-DoF approach, such as that shown in Figure 5. Then, the outer pitch angle loop is closed by designing the controller $K_\theta(s)$. It is worth noting that, following the above 2-DoF design for the pitch rate inner loop, the pre-filter $K_{\mathrm{pf,r}}$ for the pitch rate will also serve as a "shaper" (or pre-compensator) for the outer loop (see Figure 6).

5.3.1. Inner Loop (Pitch Rate)

Proceeding to the inner loop design, no outer loop is closed yet. $R_{\mathrm{Q}}(s)$ is the rate ref. input and $Q(s)$ the rate output, while the simplest plant transfer function to consider for the IMC-based design is (6), i.e., TF $Q_{\mathrm{ds2}}(s)$ reflects a close approximation of (5). This forms a rational expression overall, with the MP zero characterising a "worst case delay approximation" (original NMP zero with the original time delay included (note that, even in the case of pure time delays, at some point in the design, a rational approximation, although slightly conservative, of the time delay itself is useful. Considering this kind of approximation during the modelling for control process is an acceptable way to proceed.)). As seen from the uncompensated step response in Figure 3, the TF model $Q_{\mathrm{ds2}}(s)$ provides a worst case undershoot and overshoot characteristic

$$F(s) = \frac{1}{(\tau_0 s + 1)^2.} \tag{20}$$

The time constant τ_0 is the tunable parameter; initially setting it to the time delay (or approximated time delay) of the plant while increasing its value provides a less aggressive response. The IMC controller with $\tau_0 = 0.22$ is

$$K_{\mathrm{f}}^{[2]}(s) = \frac{0.932(1 + 0.033s + 0.0024s^2)}{s(1 + 0.073s),} \tag{21}$$

clearly in the form of an ideal PID + low-pass filter. The controller could be further simplified by a P + I equivalent if necessary, i.e., $K_{\mathrm{f-PI}}^{[2]}(s) = \frac{0.932(1+0.033s)}{s}$. Figure 13, shows

the Bode plot for $K_{\mathrm{f}}^{[2]}(s)$ and its P+I approximate. Following the procedure to obtain the pre-filter and feedforward portions, with $F_r = \frac{1}{(0.22s+1)^2}$, these are given by:

$$K_{\mathrm{ff,r}}^{[2]}(s) = \frac{0.616(1 + 0.033s + 0.0024s^2)}{(1 + 0.22s)^2} \tag{22}$$

$$K_{\mathrm{pf,r}}^{[2]}(s) = \frac{(1 - 0.22s)}{(1 + 0.22s)^2} \tag{23}$$

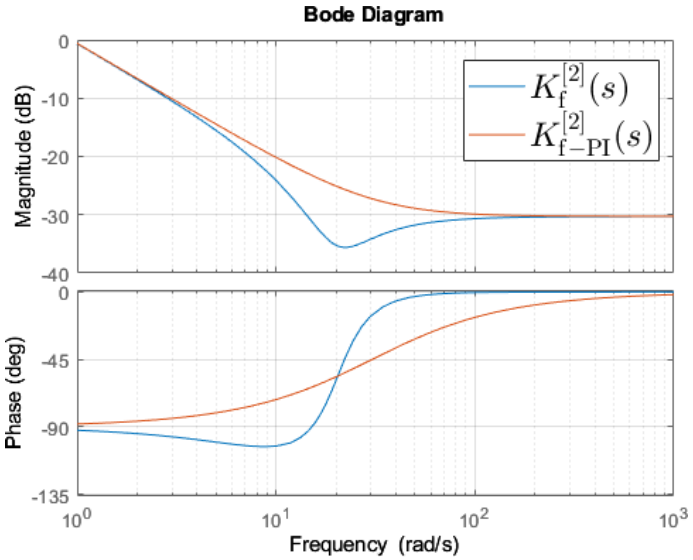

Figure 13. Inner loop feedback controller (and its approximation).

5.3.2. Outer Loop (Pitch Angle)

With the inner loop closed, the TF model used for the design of the outer loop is simply $\Theta(s)/R_{\mathrm{Q}}(s)$. While there are alternative ways to proceed, i.e., exploring outer loop controllers of increasing complexity, this simpler approach is the most beneficial.

Note that for the pitch rate inner loop, under assumption of "perfect control" and no disturbance excitation, $Q(s) \approx K_{\mathrm{pf,r}} R_{\mathrm{Q}}(s)$. Hence, one could approximate the plant model (with inner loop closed) for the design of the pitch angle outer loop by

$$\tilde{\Theta}(s) = \frac{(1 - 0.22s)}{s(1 + 0.22s)^2} R_{\mathrm{Q}}(s) \approx \frac{e^{-0.22s}}{s(1 + 0.22s)} R_{\mathrm{Q}}(s). \tag{24}$$

The above approximation allows us to perform a much simpler IMC-based design as well (this is explained later in this section and maintains minimal TF order). Here, we present two outer loop controllers, i.e., a simple (1-DoF) loop shaping controller, and a (2-DoF) IMC-based controller.

Outer Loop Simplest (1-DoF Loop Shaping)

The simplest approach to design the outer loop controller $K_{\Theta}(s)$ is by straightforward loop shaping using (24) and no feedforward. The uncompensated (outer) open loop frequency response is shown in Figure 14a.

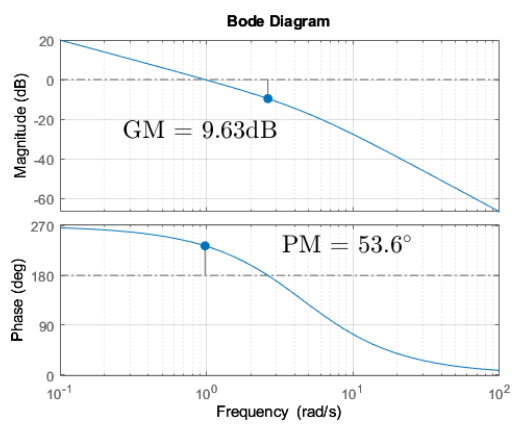

(**a**) Uncompensated OL frequency response for outer loop (pitch angle) control design

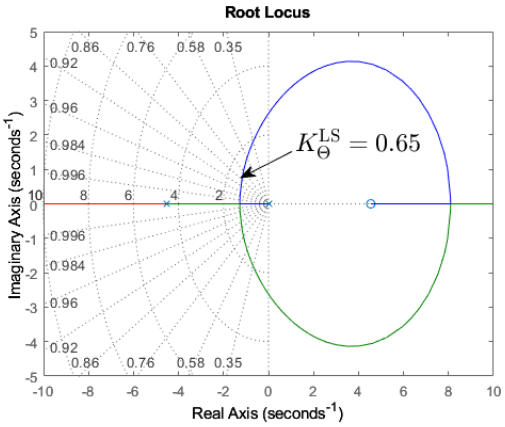

(**b**) Root locus (selected controller gain)

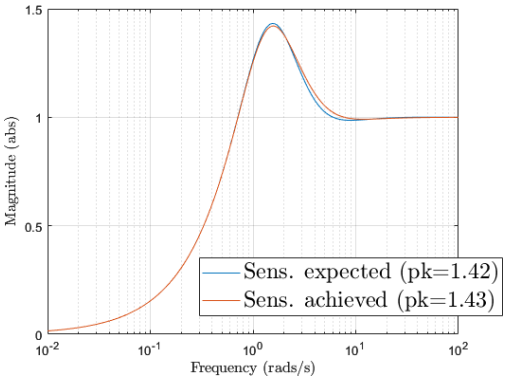

(**c**) Pitch angle sens. mag. plot.

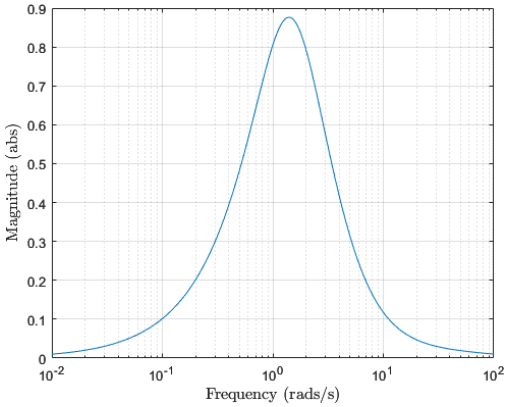

(**d**) Pitch angle sensitivity (to dist. η).

Figure 14. UAV pitch angle loop responses in frequency domain (loop shaping).

Outer Loop 2-DoF IMC-Based

The plant approximation utilised here is that of

$$\frac{\tilde{\Theta}(s)}{R_{\mathrm{Q}}(s)} = \frac{e^{-0.22s}}{s(1+0.22s)}.$$

Following the IMC procedure described in this paper, a phase-advance controller is designed, i.e.,

$$K'_{\Theta}(s) = \frac{1.136(1+0.22s)^2}{(1+0.165s+0.012s^2)}$$

with the IMC filter selected as $F = \frac{1}{(0.22s+1)^2}$. In fact, the controller $K'_{\Theta}(s)$ above can be easily approximated by

$$K'_{\Theta,\mathrm{red}}(s) = \frac{1.143(1+0.4s)}{(1+0.1s)}.$$

For completeness, and following the procedure to obtain the outer loop pre-filter and feedforward portions, with $F_r = \frac{1}{(0.5s+1)^2}$, these are given by:

$$K^{\Theta}_{\mathrm{ff,r}}(s) = \frac{s+0.22s^2}{(1+0.5s)^2}; \quad K^{\Theta}_{\mathrm{pf,r}}(s) = \frac{(1-0.22s)}{(1+0.5s)^2}. \tag{25}$$

Recall that the above choice of pre-filter ensures independent feedback and feedforward controller design. The rationale for the IMC filter selection here is to smooth the undershoot

(by allowing a slightly larger settling time). Note that, again, under perfect control, the pitch angle output is expected to adhere to $Q(s) \approx K^{\Theta}_{\text{pf,r}} R_{\Theta}(s)$.

6. Results and Discussion

The following controllers are presented here for testing, comparison and contrast purposes: **IMC–s** (IMC controller single loop, Section 5.2); **IMC–i** (IMC controller with inner loop, Section 5.3); **LS–i** (Simple loop shaping with inner loop, Section 5.3.2); and **PFCD** (Parallel Feedback Control Design [22].

For time domain simulation, the pitch angle reference is a step of amplitude $\frac{\pi}{6}$ rads, the disturbance η is a step with amplitude -0.05 rad/s (at time 3.5 s), and the disturbance ρ is a step with amplitude $-0.2\frac{\pi}{6}$ rads (as time 4.5 s). The controllers presented in this paper were tested on the original model of the UAV setup. In the simulation, when disturbances apply, these act independently.

Figure 15 reports the pitch angle and pitch rate signals for the scheme with the simplest loop-shaping (1-DoF) outer loop controller. Figure 16 presents the pitch angle and pitch rate signals for the scheme with 2-DoF IMC-based outer loop controller. In both cases, an IMC-based inner loop applies, as discussed earlier. One can clearly see the disturbance rejection performance in both cases. The time domain response for the PFCD scheme is shown in Figure 7, and while the pitch angle and pitch rate signals show smooth responses, the scheme does not offer appropriate disturbance rejection (especially to pitch rate disturbance). In addition, there is a very small pitch angle steady-state offset remaining. The PFCD scheme could be improved (especially in terms of disturbance rejection) with the use of more complex controller structure and use of optimisation; however, this would further impact its simplicity compared with the IMC-based solutions.

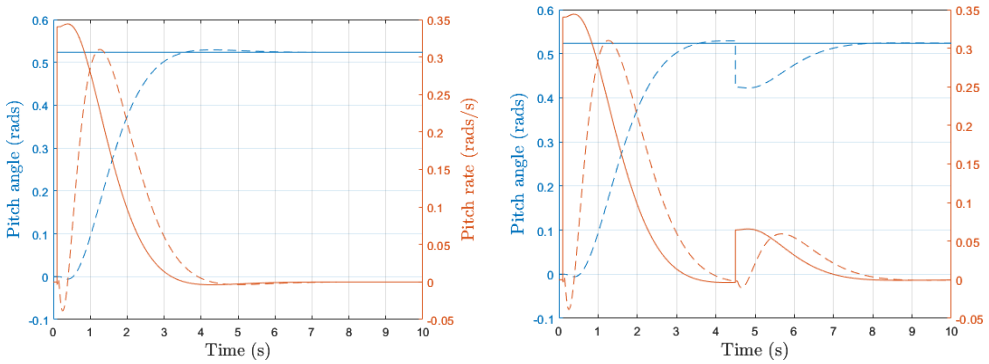

(**a**) no disturbances (**b**) disturbance on pitch angle

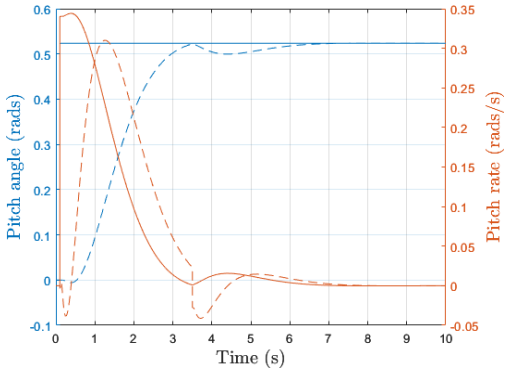

(**c**) disturbance on pitch rate

Figure 15. LS–i time domain performance.

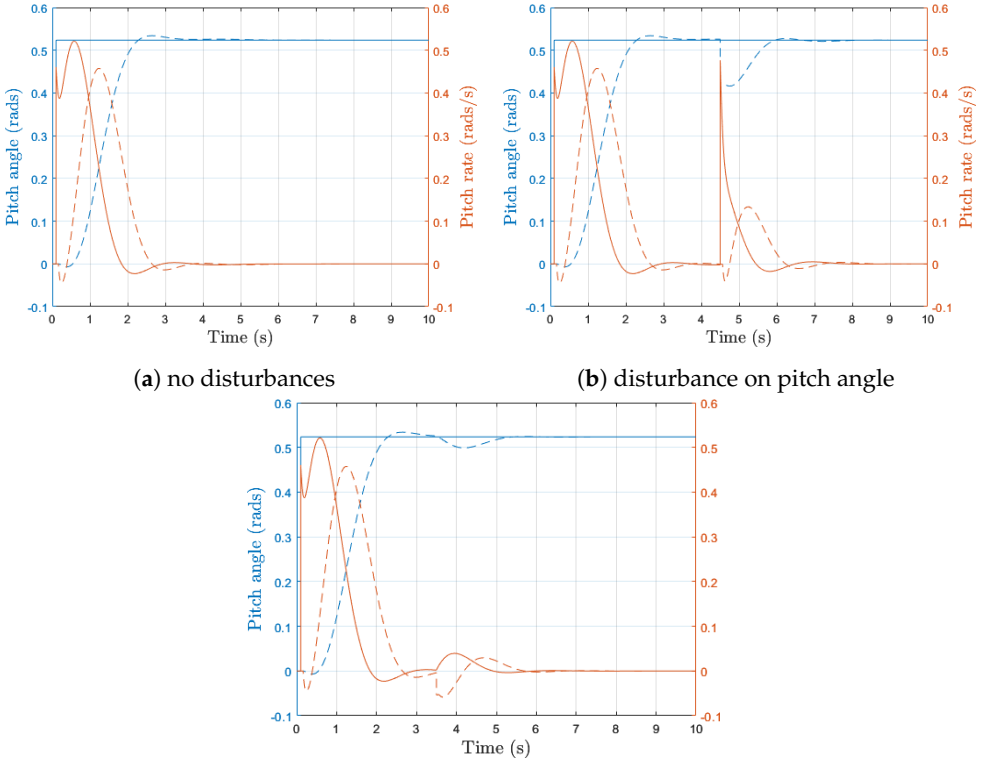

(**a**) no disturbances (**b**) disturbance on pitch angle

(**c**) disturbance on pitch rate

Figure 16. IMC–i outer loop control responses in time domain.

The 1-DoF loop-shaping outer loop controller is more conservative than the 2-DoF IMC-based outer loop controller scheme, and hence, offers slightly better robustness properties, as seen in Figure 17. The 2-DoF IMC-based outer loop controller scheme takes advantage of the IMC feedback controller structure and the feedforward controller to offer a more aggressive, yet acceptably robust outcome. Figure 18 shows the IMC-based feedback controller's frequency response (and its simplification) and the achieved disturbance rejection to the pitch rate η disturbance channel.

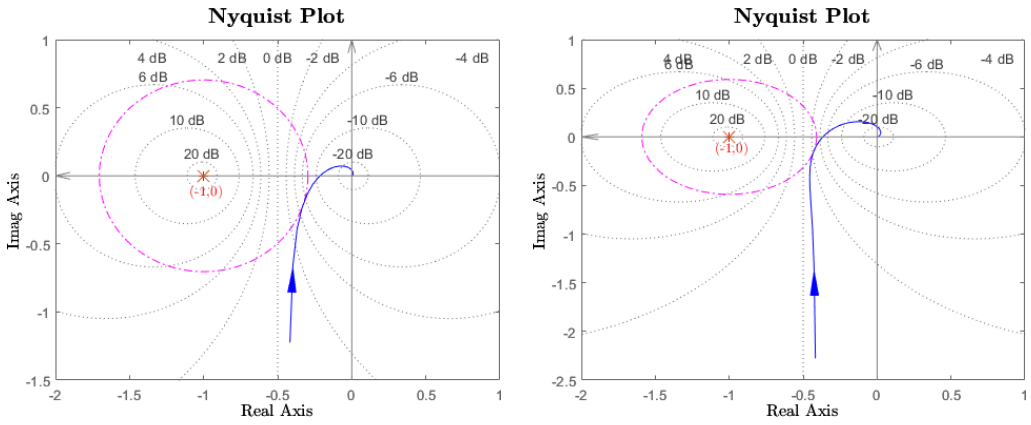

(**a**) Loop shaping (**LS–i**) (**b**) IMC-based (**IMC–i**)

Figure 17. Nyquist plots for pitch angle control loop (robustness).

Moreover, the proposed controller schemes offer better noise rejection properties as shown by the complementary sensitivity plot in Figure 19a (on the pitch angle channel), compared with PFCD. Note that we assess high frequency noise rejection via frequency responses, i.e., design closed-loop TF. We have not included noisy time domain responses in order to illustrate the deterministic disturbance rejection more clearly. Figure 19b illustrates

the control input (control effort); clearly, the proposed controller schemes maintain smooth control (elevons) effort very comparable to that of PFCD.

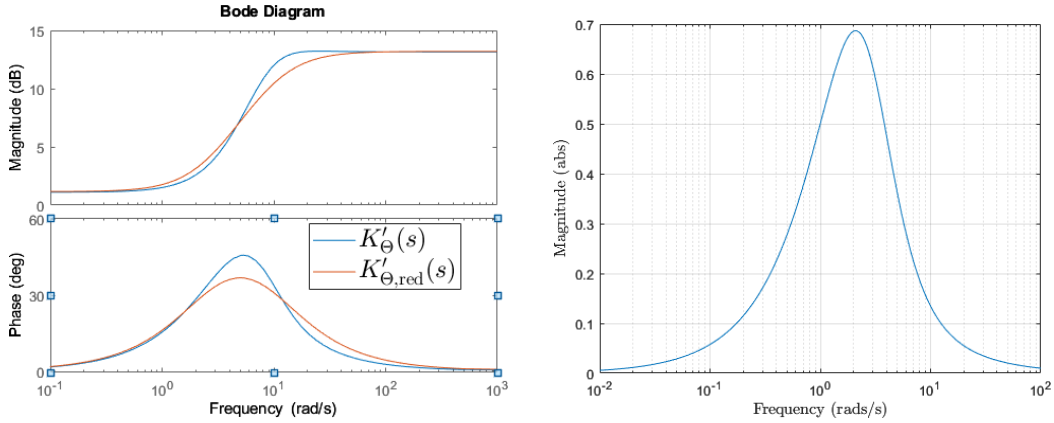

(**a**) IMC controller and its reduced version (**b**) Sensitivity to dist. η

Figure 18. IMC–i controller (frequency response).

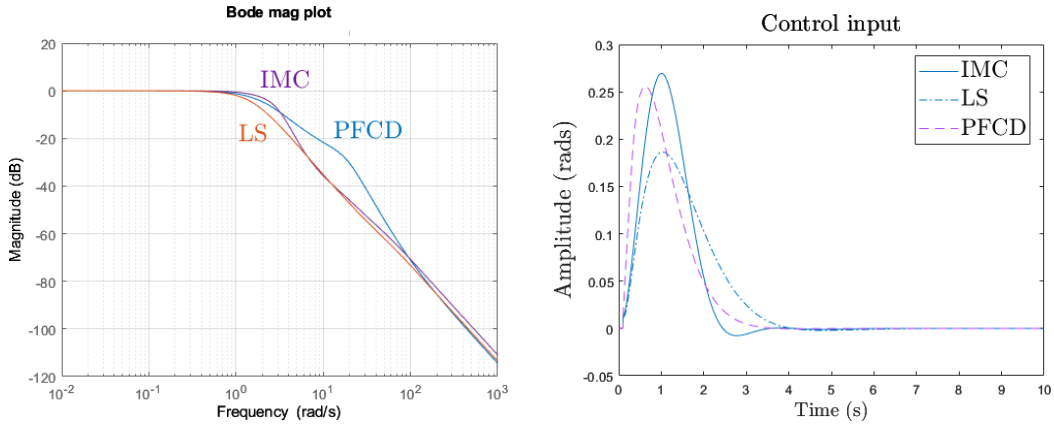

(**a**) Complementary sensitivity (noise rejection performance, frequency response) (**b**) Control input (all schemes, no disturbances, time domain)

Figure 19. UAV pitch angle loop (with rate feedback closed) performance.

The controller's performance is summarised in a detailed set of performance metrics shown in Table 2, which also lists the single-loop IMC-based controller, for completeness (however, we mainly concentrate on the schemes with closed inner loops, for a fairer comparison with PFCD). From the viewpoint of controller structure setup, the proposed controllers offer explainability relative to the UAV system dynamics, unlike PFCD.

The following important points are highlighted:

- The IMC-based controller design for the inner loop (pitch rate) serves as a shaper for the outer loop controller design, both for the simplest loop-shaping approach and for the 2-DoF IMC-based outer loop controller approach. In particular, the pre-filter $K_{\mathrm{pf,r}}$ offers a "virtual" simplified plant TF (under an assumption of perfect control) for the outer loop controller's design.
- The plant TF model representation (so-called 'modelling for control') for the IMC-based control design process leads to explainable controller structure (i.e., PID-type, phase-advance type, etc.), and further simplification of the controllers can be achieved by straightforward investigation of their characteristics (as shown in this paper).
- The IMC-based controller design does not necessitate complex optimisation (although it is possible to follow more rigorous optimisation for more complex TF structures).

Table 2. Evaluation of controller schemes *.

	Controller Schemes			
Metrics	**IMC–s**	**IMC–i**	**LS–i**	**PFCD**
T_s (settling time, sec)	2.19	**2.168**	3.21	2.641
Undershoot peak	−0.07	−0.007	**−0.006**	−0.02
Overshoot peak	**0.5236**	0.534	0.529	0.525
T_{zc} (zero cross time, sec)	**0.4**	0548	0.539	0.491
Disturbance rejection (det.)	Y	Y	Y	N
Sensitivity peak (abs)	1.81	1.69	1.42	**1.4**
s.s. error (tracking)	0	0	0	≈ 0

* Response to pitch angle reference command of $\pi/6$ rad. IMC–s (Section 5.2); IMC–i (Section 5.3); LS–i (Section 5.3.2); PFCD (Section 4.3) Zero crossing time: curve crosses x-axis from `-ve` to `+ve` (and remains in `+ve`). Disturbance rejection (deterministic) achieved or not (to all disturbances). Tracking achieved under no disturbances (last row).

7. Conclusions

This paper presents a structured control design for a fixed-wing UAV platform with non-minimum phase (NMP) zero characteristics, using the Internal Model Control (IMC) design. The resulting IMC-based controller offers a simple and explainable (in terms of the controller structure's linkage to the system performance) controller without the need for complex optimisation. This approach is highly relevant to practical applications in NMP-type UAV control problems, as it takes advantage of the model's NMP zero characteristics to inform the design process and can also enable fine loop-shaping with higher-order model representations.

The proposed IMC-based controllers outperform a recently proposed PFCD-proposed scheme for the same UAV platform, offering better disturbance rejection while maintaining comparable robustness properties (even if the model for control used is a simple approximation of the original model). This approach can serve as a baseline controller for further structured control design optimisation for UAV control, and can also serve as a baseline "shaping filter" for more advanced robust control designs, such as H-infinity methods.

Key points of the proposed IMC-based UAV-targeted control solution include: (i) its simplicity and avoidance of complex optimisation, (ii) its structured model-based approach that incorporates NMP zero characteristics of the UAV platform in the control design, (iii) its comparable performance to that of PFCD while offering superior disturbance rejection.

Rigorous simulations and analysis demonstrate the efficacy of the proposed approach, while the paper also recommends ways to represent the transfer function model of the UAV platform for control design purposes and how these relate to the system performance. This approach offers a valuable tool to industrial UAV control practitioners and applied researchers working on UAV controller design problems.

Funding: This research received no external funding.

Data Availability Statement: Results can be duplicated directly from data information provided in the article. Data sharing is not applicable to this article.

Conflicts of Interest: The authors declare no conflict of interest.

Abbreviations

The following abbreviations are used in this manuscript:

SISO	Single-Input–Single-Output
NMP	Non-minimum phase
TF	Transfer function
CL, OL	Closed-loop, Open-loop
DoF	Degree of Freedom

FDBK	Feedback
IMC	Internal Model Control
PFCD	Parallel Feedback Control Design
UAV	Unmanned Aerial Vehicle
GM, GRM	Gain margin, Gain reduction margin
PM, PRM	Phase margin, Phase reduction margin

References

1. Hoagg, J.B.; Bernstein, D.S. Nonminimum-phase zeros-much to do about nothing-classical control-revisited part II. *IEEE Control Syst. Mag.* **2007**, *27*, 45–57. [CrossRef]
2. Storkaas, E.; Skogestad, S. Controllability Analysis of an Unstable, Non-Minimum Phase Process. In Proceedings of the 16th IFAC World Congress, Prague, Czech Republic, 3–8 July 2005; Volume 38, pp. 592–597. [CrossRef]
3. Theodoulis, S.; Proff, M. Robust Flight Control Tuning for Highly Agile Missiles. In Proceedings of the AIAA Scitech 2021 Forum, Online, 11–15 & 19–21 January 2021. [CrossRef]
4. Li, J.H.; Kang, H.; Kim, M.G.; Lee, M.J.; Cho, G.R. Asymptotic Trajectory Tracking of Underactuated Non-Minimum Phase Marine Vessels. *IFAC–PapersOnLine* **2022**, *55*, 281–286. [CrossRef]
5. Hassan, F.; Zolotas, A. Impact of fractional order methods on optimized tilt control for rail vehicles. *Fract. Calc. Appl. Anal.* **2017**, *20*, 765–789. [CrossRef]
6. Åström, K. Limitations on Control System Performance. *Eur. J. Control* **2000**, *6*, 2–20. [CrossRef]
7. Schweiger, K.; Preis, L. Urban Air Mobility: Systematic Review of Scientific Publications and Regulations for Vertiport Design and Operations. *Drones* **2022**, *6*, 179. [CrossRef]
8. Alsamhi, S.H.; Shvetsov, A.V.; Kumar, S.; Hassan, J.; Alhartomi, M.A.; Shvetsova, S.V.; Sahal, R.; Hawbani, A. Computing in the Sky: A Survey on Intelligent Ubiquitous Computing for UAV-Assisted 6G Networks and Industry 4.0/5.0. *Drones* **2022**, *6*, 177. [CrossRef]
9. Shakeel, T.; Arshad, J.; Jaffery, M.H.; Rehman, A.U.; Eldin, E.T.; Ghamry, N.A.; Shafiq, M. A Comparative Study of Control Methods for X3D Quadrotor Feedback Trajectory Control. *Appl. Sci.* **2022**, *12*, 9254. [CrossRef]
10. Safwat, E.; Zhang, W.; Mohsen, A.; Kassem, M. Design and Analysis of a Robust UAV Flight Guidance and Control System Based on a Modified Nonlinear Dynamic Inversion. *Appl. Sci.* **2019**, *9*, 3600. [CrossRef]
11. Wang, H.; Li, Z.; Xiong, H.; Nian, X. Robust H-infinity attitude tracking control of a quadrotor UAV on SO(3) via variation-based linearization and interval matrix approach. *ISA Trans.* **2019**, *87*, 10–16. [CrossRef]
12. Sir Elkhatem, A.; Engin, S.N.; Pasha, A.A.; Rahman, M.M.; Pillai, S.N. Robust Control for Non-Minimum Phase Systems with Actuator Faults: Application to Aircraft Longitudinal Flight Control. *Appl. Sci.* **2021**, *11*, 11705. [CrossRef]
13. Yang, J.H.; Xu, H.K. Robust Controller Design for Non-Minimum Phase UAV System and System Analysis. *IEEE Access* **2018**, *6*, 70734–70769. [CrossRef]
14. Li, Y.; Qin, Y.; Xu, W.; Zhang, F. Modeling, Identification, and Control of Non-minimum Phase Dynamics of Bi-copter UAVs. In Proceedings of the 2020 IEEE/ASME International Conference on Advanced Intelligent Mechatronics (AIM), Boston, MA, USA, 6–9 July 2020; pp. 1249–1255. [CrossRef]
15. Saxena, S.; Hote, Y.V. Advances in internal model control technique: A review and future prospects. *IETE Tech. Rev.* **2012**, *29*, 461–472. [CrossRef]
16. Chiu, M.S.; Arkun, Y. Parametrization of all stabilizing IMC controllers for unstable plants. *Int. J. Control* **1990**, *51*, 329–340. [CrossRef]
17. Rivera, D.E.; Flores, M.E. Internal model control. *Control Syst. Robot. Autom.* **2009**, *2*, 80–108.
18. Zhou, K. A natural approach to high performance robust control: Another look at Youla parameterization. In Proceedings of the SICE 2004 Annual Conference, Sapporo, Japan, 4–6 August 2004; Volume 1, pp. 869–874.
19. Balestrieri, E.; Daponte, P.; De Vito, L.; Picariello, F.; Tudosa, I. Sensors and Measurements for UAV Safety: An Overview. *Sensors* **2021**, *21*, 8253. [CrossRef] [PubMed]
20. Valavanis, K.P.; Vachtsevanos, G.J. (Eds.) *Handbook of Unmanned Aerial Vehicles*; Springer: Dordrecht, The Netherlands, 2015. [CrossRef]
21. Šoberl, D.; Bratko, I.; Žabkar, J. Learning to Control a Quadcopter Qualitatively. *J. Intell. Robot. Syst.* **2020**, *100*, 1097–1110. [CrossRef]
22. Pukacz, A.; Kabziński, J. Control of Unmanned Aerial Vehicles with Non-Minimum Phase Dynamics Using Parallel Differential Compensation. In Proceedings of the 2022 26th International Conference on Methods and Models in Automation and Robotics (MMAR), Miedzyzdroje, Poland, 22–25 August 2022; pp. 70–75. [CrossRef]
23. Saengphet, W.; Tantrairatn, S.; Thumtae, C.; Srisertpol, J. Implementation of system identification and flight control system for UAV. In Proceedings of the 2017 3rd International Conference on Control, Automation and Robotics (ICCAR), Nagoya, Japan, 22–24 April 2017; pp. 678–683. [CrossRef]
24. Skogestad, S. Simple analytic rules for model reduction and PID controller tuning. *J. Process Control* **2003**, *13*, 291–309. [CrossRef]
25. Bequette, B.W. *Process Control: Modeling, Design, and Simulation*; Prentice Hall Professional: Upper Saddle River, NJ, USA, 2003.

26. Lang, G.; Ham, J. Conditional feedback systems-A new approach to feedback control. *Trans. Am. Inst. Electr. Eng. Part II Appl. Ind.* **1955**, *74*, 152–161. [CrossRef]
27. Faanes, A.; Skogestad, S. Feedforward control under the presence of uncertainty. *Eur. J. Control* **2004**, *10*, 30–46. [CrossRef]
28. Noury, K.; Yang, B. Analytical Statistical Study of Linear Parallel Feedforward Compensators for Nonminimum-Phase Systems. In Proceedings of the Dynamic Systems and Control Conference, Park City, UT, USA, 8–11 October 2019; Volume 1. [CrossRef]
29. Wang, Q.G.; Hang, C.C.; Yang, X.P. Single-loop controller design via IMC principles. *Automatica* **2001**, *37*, 2041–2048. [CrossRef]
30. Bin, H.; Zheng, P.; Liang, J. Multi-loop internal model controller design based on a dynamic PLS framework. *Chin. J. Chem. Eng.* **2010**, *18*, 277–285.
31. Azar, A.T.; Serrano, F.E. Robust IMC–PID tuning for cascade control systems with gain and phase margin specifications. *Neural Comput. Appl.* **2014**, *25*, 983–995. [CrossRef]
32. Ghousiya Begum, K.; Seshagiri Rao, A.; Radhakrishnan, T. Enhanced IMC based PID controller design for non-minimum phase (NMP) integrating processes with time delays. *ISA Trans.* **2017**, *68*, 223–234. [CrossRef] [PubMed]
33. Vilanova, R.; Arrieta, O.; Ponsa, P. IMC based feedforward controller framework for disturbance attenuation on uncertain systems. *ISA Trans.* **2009**, *48*, 439–448. [CrossRef] [PubMed]
34. Chen, J.; He, Z.F.; Qi, X. A new control method for MIMO first order time delay non-square systems. *J. Process Control* **2011**, *21*, 538–546. [CrossRef]
35. De Keyser, R.; Copot, C.; Hernandez, A.; Ionescu, C. Discrete-time internal model control with disturbance and vibration rejection. *J. Vib. Control* **2017**, *23*, 3–15. [CrossRef]
36. Henson, M.A.; Seborg, D.E. An internal model control strategy for nonlinear systems. *AIChE J.* **1991**, *37*, 1065–1081. [CrossRef]
37. Ping, Z.; Wang, T.; Huang, Y.; Wang, H.; Lu, J.G.; Li, Y. Internal Model Control of PMSM Position Servo System: Theory and Experimental Results. *IEEE Trans. Ind. Informatics* **2019**, *16*, 2202–2211. [CrossRef]
38. Yang, Q.; Chi, Z.; Wang, L. Uncertainty Analysis of Suspension System Caused by Horizontal Misalignment and Its Suppression Method. *Machines* **2022**, *10*, 977. [CrossRef]
39. Rivera, D.E.; Morari, M. Internal Model Control Perspectives on Model Reduction. In Proceedings of the 1985 American Control Conference, Boston, MA, USA, 19–21 June 1985; pp. 1293–1298. [CrossRef]
40. Bouzid, Y.; Siguerdidjane, H.; Zareb, M.; Bestaoui, Y. Improved IMC-Filter Design to IMC-PI Equivalence: Application to Quadrotor. *IFAC-PapersOnLine* **2019**, *52*, 158–163. [CrossRef]
41. Olayinka, T.O.; Olatide, A.A.; Oluwagbemiga, A.D.; Okelola, M.O. Internal Model Control Tuned Proportional Integral Derivative for Quadrotor Unmanned Aerial Vehicle Dynamic Model. *Control. Theory Inform. (IISTE)* **2020**, *9*, 1–10.
42. Gao, Q.; Du, M.; Ji, Y. The controller design of quadrotor UAV based on internal model control. In Proceedings of the 2017 36th Chinese Control Conference (CCC), Dalian, China, 26–28 July 2017; pp. 505–510. [CrossRef]
43. Chen, P.; Zhang, Y.; Wang, J.; Azar, A.T.; Hameed, I.A.; Ibraheem, I.K.; Kamal, N.A.; Abdulmajeed, F.A. Adaptive Internal Model Control Based on Parameter Adaptation. *Electronics* **2022**, *11*, 3842. [CrossRef]
44. Chia, T.L.; Lefkowitz, I. Internal model-based control for integrating processes. *ISA Trans.* **2010**, *49*, 519–527. [CrossRef] [PubMed]

Simple internal model-based robust control design for a non-minimum phase unmanned aerial vehicle

Zolotas, Argyrios

2023-04-21

Zolotas A (2023) Simple internal model-based robust control design for a non-minimum phase unmanned aerial vehicle, Machines, Volume 11, Issue 4, April 2023, Article number 498
https://doi.org/10.3390/machines11040498